Reconfigurable beams with arbitrary polarization and shape distributions at a given plane

David Maluenda,[1] Ignasi Juvells,[1] Rosario Martínez-Herrero,[2] and Artur Carnicer[1,*]

[1]*Departament de Física Aplicada i Òptica, Universitat de Barcelona (UB), Martí i Franquès 1, 08028 Barcelona (Spain)*

[2]*Departamento de Óptica, Facultad de Ciencias Físicas, Universidad Complutense de Madrid, 28040 Madrid (Spain)*

[*]*artur.carnicer@ub.edu*

Abstract: Methods for generating beams with arbitrary polarization based on the use of liquid crystal displays have recently attracted interest from a wide range of sources. In this paper we present a technique for generating beams with arbitrary polarization and shape distributions at a given plane using a Mach-Zehnder setup. The transverse components of the incident beam are processed independently by means of spatial light modulators placed in each path of the interferometer. The modulators display computer generated holograms designed to dynamically encode any amplitude value and polarization state for each point of the wavefront in a given plane. The steps required to design such beams are described in detail. Several beams performing different polarization and intensity landscapes have been experimentally implemented. The results obtained demonstrate the capability of the proposed technique to tailor the amplitude and polarization of the beam simultaneously.

OCIS codes: (260.5430) Polarization; (090.1760) Computer holography; (070.6120) Spatial light modulators.

References

1. Q. Zhan, "Cylindrical vector beams: from mathematical concepts to applications," Adv. Opt. Photonics **1**, 1–57 (2009).
2. S.C. Tidwell, G.H. Kim, and W.D. Kimura, "Efficient radially polarized laser beam generation with a double interferometer," Appl. Opt. **32**, 5222–5229 (1993).
3. M.A.A. Neil, F. Massoumian, R. Juškaitis, and T. Wilson, "Method for the generation of arbitrary complex vector wave fronts," Opt. Lett. **27**, 1929–1931 (2002).
4. K.C. Toussaint Jr, S.P. Park, J.E. Jureller, and N.F. Scherer, "Generation of optical vector beams with a diffractive optical element interferometer," Opt. Lett. **30**, 2846–2848 (2005).
5. A. Flores-Pérez, J. Hernández-Hernández, R. Jáuregui, and K. Volke-Sepúlveda, "Experimental generation and analysis of first-order TE and TM Bessel modes in free space," Opt. Lett. **31**, 1732–1734 (2006).
6. J.A. Davis, D.E. McNamara, D.M. Cottrell, and T. Sonehara, "Two-dimensional polarization encoding with a phase-only liquid-crystal spatial light modulator," Appl. Opt. **39**, 1549–1554 (2000).
7. R.L. Eriksen, P.C. Mogensen, and J. Glückstad, "Elliptical polarisation encoding in two dimensions using phase-only spatial light modulators," Opt. Commun. **187**, 325–336 (2001).
8. C. Maurer, A. Jesacher, S. Fürhapter, S. Bernet, and M. Ritsch-Marte, "Tailoring of arbitrary optical vector beams," New J. Phys. **9**, 78 (2007).
9. X.L. Wang, J. Ding, W.J. Ni, C.S. Guo, and H.T. Wang, "Generation of arbitrary vector beams with a spatial light modulator and a common path interferometric arrangement," Opt. Lett. **32**, 3549–3551 (2007).

#183193 - $15.00 USD Received 17 Jan 2013; revised 15 Feb 2013; accepted 15 Feb 2013; published 26 Feb 2013

10. H. Chen, Z. Zheng, B.F. Zhang, J. Ding, and H.T. Wang, "Polarization structuring of focused field through polarization-only modulation of incident beam," Opt. Lett. **35**, 2825–2827 (2010).
11. H.T. Wang, X.L. Wang, Y. Li, J. Chen, C.S. Guo, and J. Ding, "A new type of vector fields with hybrid states of polarization," Opt. Express **18**, 10786–10795 (2010).
12. H. Chen, J. Hao, B.F. Zhang, J. Xu, J. Ding, and H.T. Wang, "Generation of vector beam with space-variant distribution of both polarization and phase," Opt. Lett. **36**, 3179–3181 (2011).
13. I. Moreno, C. Iemmi, J. Campos, and M.J. Yzuel, "Jones matrix treatment for optical fourier processors with structured polarization," Opt. Lett. **19**, 4583–4594 (2011).
14. S. Tripathi and K.C. Toussaint, "Versatile generation of optical vector fields and vector beams using a non-interferometric approach," Opt. Lett. **20**, 10788–10795 (2012).
15. S. Liu, P. Li, T. Peng, and J. Zhao, "Generation of arbitrary spatially variant polarization beams with a trapezoid sagnac interferometer," Opt. Express **20**, 21715–21721 (2012).
16. F. Kenny, D. Lara, O.G. Rodríguez-Herrera, and C. Dainty, "Complete polarization and phase control for focus-shaping in high-NA microscopy," Opt. Express **20**, 14015–14029 (2012).
17. R. Tudela, E. Martin-Badosa, I. Labastida, S. Vallmitjana, and A. Carnicer, "Wavefront reconstruction by adding modulation capabilities of two liquid crystal devices," Opt. Eng. **43**, 2650–2657 (2004).
18. V. Arrizón, "Complex modulation with a twisted-nematic liquid-crystal spatial light modulator: double-pixel approach," Opt. Lett. **28**, 1359–1361 (2003).
19. V. Arrizón, L. González, R. Ponce, and A. Serrano-Heredia, "Computer-generated holograms with optimum bandwidths obtained with twisted-nematic liquid-crystal displays," Appl. Opt. **44**, 1625–1634 (2005).
20. E. Martín-Badosa, A. Carnicer, I. Juvells, and S. Vallmitjana, "Complex modulation characterization of liquid crystal devices by interferometric data correlation," Meas. Sci. Technol. **8**, 764–772 (1997).
21. M. Born and E. Wolf, *Principles of Optics: Electromagnetic Theory of Propagation, Interference and Diffraction of Light* (Cambridge University Press, 1999).

1. Introduction

The propagation of polarized light and its interaction with matter have been extensively explored in the fields of optical inspection and meteorology, display technologies, data storage, optical communications, material sciences and astronomy, as well as in biological research [1]. While early studies mainly dealt with spatially homogeneous polarization states, in recent years interest in arbitrary spatially-variant polarized beams (ASPBs) has increased significantly due to their special properties compared to homogeneously polarized beams, which can thereby enhance the functionality of optical systems. Nevertheless, the generation of ASPBs can be a difficult task; while static techniques do not allow dynamic encoding of ASPB patterns [2–5], a solution can be found using spatial light modulators (SLMs) which can be considered as reconfigurable phase retarder devices controlled by computer [6–16].

In this paper we present a method for generating beams with arbitrary polarization and shape distributions (BAPS) at a given plane. Our approach is based on a Mach-Zehnder setup combined with a translucent SLM in each path of the interferometer [17]. The transverse components of the incident light beam are processed independently and modified by means of specifically designed holograms calculated using a procedure derived from Arrizón's method to encode complex signals [18, 19]. The processed transverse components are recombined and imaged on a CCD camera. Our approach allows us to encode any polarization state at each point of the wavefront and the amplitude may also be modeled so as to obtain a particular shape in a given plane.

The paper is organized as follows: in section 2 we present the optical setup required to generate BAPS, while the algorithm for calculating complex-valued holograms is reviewed in section 3. Several examples of experimentally generated BAPS that illustrate how this method is used in practice are found in section 4. Finally, the conclusions are summarized in section 5.

2. Optical setup

Figure 1 shows the experimental setup based on a Mach-Zehnder interferometer. An unpolarized HeNe laser beam passes trough linear polarizer P_1 set at 45° with respect to the *x* direction;

#183193 - $15.00 USD Received 17 Jan 2013; revised 15 Feb 2013; accepted 15 Feb 2013; published 26 Feb 2013

this field ($\mathbf{E}_{in}$) is described by $\mathbf{E}_{in} = E_{in2}(x,y)\,\mathbf{e}_1 + E_{in1}(x,y)\,\mathbf{e}_2$, where $\mathbf{e}_1$ and $\mathbf{e}_2$ are unit vectors in the x and y directions. Later, $\mathbf{E}_{in}$ is split into two beams by means of a polarizing beam splitter, PBS_1. Reflected by mirror M_1 or M_2, the split beams pass through different wave plates which rotate the oscillating plane and set the modulator in order to achieve the desired modulation curve. Afterwards, the light passes through modulator SLM_1 or SLM_2 which display complex transmittances $h_1(x,y)$ and $h_2(x,y)$, respectively. Each of the displays used is a translucent twisted nematic Holoeye HEO 0017 with a resolution of 1024×768 pixels and $32\,\mu m$ of pixel pitch. Then, the light is recombined by means of the second polarizing beam splitter PBS_2 and fed into the on-axis reconstruction system consisting of a $4f$-Fourier lens system. Note that a spatial filter in the back focal plane of L_1 is needed to remove higher-order diffracted terms generated by the holograms $h_1(x,y)$ and $h_2(x,y)$. Finally, the resulting field is analyzed by means of P_2 and the final irradiance is recorded by the CCD camera. The output field ($\mathbf{E}_{out}(x,y)$) at the camera plane is

$$\begin{aligned} \mathbf{E}_{out}(x,y) &= E_{in1}(x,y)\,h_1(x,y)\mathbf{e}_1 + E_{in2}(x,y)\,h_2(x,y)\mathbf{e}_2 = \\ &= A_1(x,y)\exp(i\phi_1(x,y))\mathbf{e}_1 + A_2(x,y)\exp(i\phi_2(x,y))\mathbf{e}_2\,. \end{aligned} \tag{1}$$

Where $A_1(x,y)$ and $A_2(x,y)$ are the amplitude distributions of $\mathbf{E}_{out}(x,y)$ in the x and y directions respectively and $\phi_1(x,y)$ and $\phi_2(x,y)$ are the corresponding accumulated phase shifts. The total phase delay between components x and y of $\mathbf{E}_{out}(x,y)$ is $\phi(x,y) = \phi_2(x,y) - \phi_1(x,y)$. For convenience, we write $A_1(x,y) = A_{sh}(x,y)a_1(x,y)$ and $A_2(x,y) = A_{sh}(x,y)a_2(x,y)$ with $a_1^2(x,y) + a_2^2(x,y) = 1$, where $A_{sh}(x,y)$ is the beam shape distribution. In this way, the oscillation orientation distribution at each point (x,y) of the wavefront is $\theta(x,y) = \tan^{-1}(a_2(x,y)/a_1(x,y))$. For simplicity, the magnification introduced by the imaging $4f$ system is not taken into account.

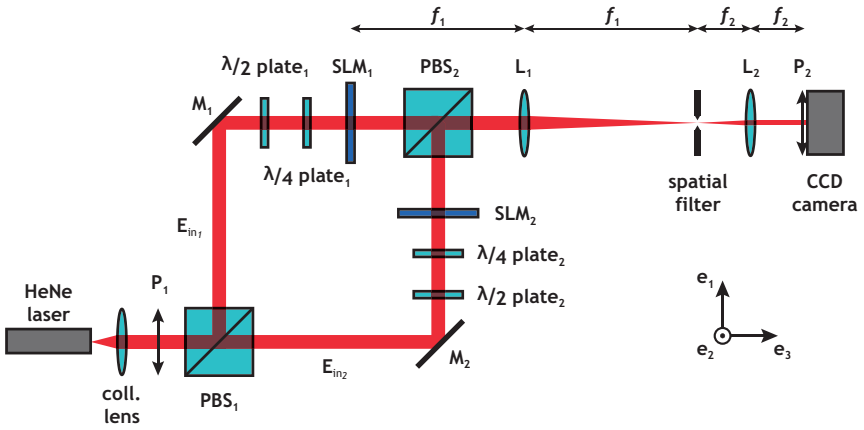

Fig. 1: Sketch of the experimental setup.

3. Codification procedure

Arrizón developed a cell-based holographic algorithm for encoding complex optical signals in SLMs with arbitrary amplitude and phase distributions [19]. Here, we briefly summarize the steps required to generate holograms able to shape the amplitude and the phase of the wavefront. Figure 2(a) is a polar diagram of the set of complex values accessible by modulators SLM_1 (blue dots) and SLM_2 (red dots). Both curves have been determined using the method

#183193 - $15.00 USD Received 17 Jan 2013; revised 15 Feb 2013; accepted 15 Feb 2013; published 26 Feb 2013

presented in [20], which is appropriate for transmissive twisted-nematic modulators. The wave plates are oriented as follows: SLM_1, $\lambda/2$ at 70° and $\lambda/4$ at 145°; SLM_2, $\lambda/2$ at 150° and $\lambda/4$ at 35° (these angles are from the fast axis of the wave-plate). From Fig. 2(a) it is apparent that: (i) the amplitude modulation is not constant and no phase-only modulation would be possible using this device; (ii) the phase values are limited to the range [0°, 240°]; and (iii) the displays perform in similar but not identical ways. Note that the phase origin of SLM_2 is shifted by fine tuning the optical path of the corresponding arm of the interferometer. The

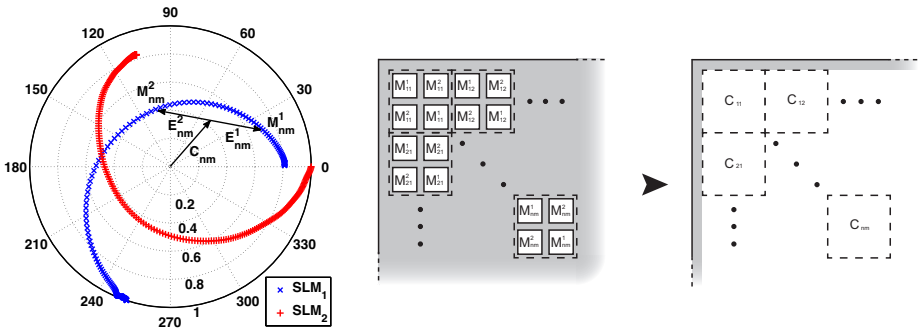

Fig. 2: (a) Modulation response M for the Holoeye displays SLM_1 and SLM_2. The Fig. also shows how C_{nm} can be accessed as a combination of $M^{(1)}_{nm}$, $M^{(2)}_{nm}$, $E^{(1)}_{nm}$ and $E^{(2)}_{nm}$. (b) Double pixel hologram approach: four pixels of the SLM that have values $M^{(1)}_{nm}$ and $M^{(2)}_{nm}$ are required to encode each complex value, C_{nm}.

holographic algorithm takes advantage of the amplitude-phase coupling of these displays to achieve full-complex modulation with two SLMs. Let C_{nm} be the complex value to be coded at position (n,m). If C_{nm} does not belong to the modulation curve M, it can be written as $C_{nm} = M^{(1)}_{nm} - E^{(1)}_{nm}$ and $C_{nm} = M^{(2)}_{nm} - E^{(2)}_{nm}$ where $M^{(1)}_{nm}$ and $M^{(2)}_{nm}$ are points on M (see Fig. 2(a) for details). Selecting $M^{(1)}_{nm}$ and $M^{(2)}_{nm}$ in such a way that $E^{(1)}_{nm} = -E^{(2)}_{nm}$ then $C_{nm} = \left(M^{(1)}_{nm} + M^{(2)}_{nm}\right)/2$. Following the cell-oriented holograms approach, four pixels in the SLM are required to encode each complex value, C_{nm}, as depicted in Fig. 2(b). Using this pixel arrangement, the optical Fourier transforms of $M^{(1)}_{nm}$ and $M^{(2)}_{nm}$ are reconstructed on-axis whereas the undesired terms E^1_{nm} and E^2_{nm} are diffracted off-axis; to remove their contribution, a spatial filter is placed at the back focal plane of lens L_1. Finally, the desired distribution is reconstructed on-axis at the back focal plane of lens L_2 (CCD plane).

Figure 3 shows all the possible values for C_{nm} that can be obtained as a combination of two points $M^{(1)}_{nm}$ and $M^{(2)}_{nm}$ that belong to the modulation curves. Blue and red dots indicate the points of the complex plane that can be accessed by SLM_1 or SLM_2, respectively. Consequently, if the phase origin of SLM_2 is shifted 60° with respect to the other display, the system can access any amplitude value and phase difference $\phi(x,y)$ between the two components within the circle of transmittance $T = 0.4$. Although the relative phase delay, $\phi(x,y)$, can be achieved from many pairs $\phi_1(x,y)$ and $\phi_2(x,y)$, it is necessary to emphasize that this pair of phase distributions has to be smooth and without phase jumps across the beam.

#183193 - $15.00 USD Received 17 Jan 2013; revised 15 Feb 2013; accepted 15 Feb 2013; published 26 Feb 2013

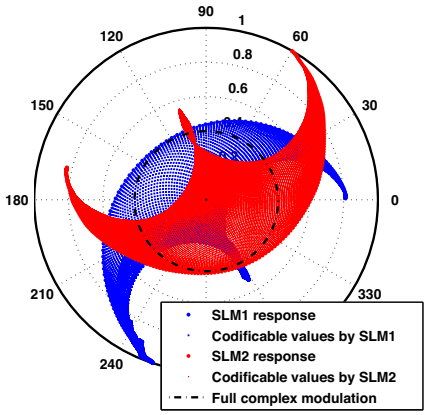

Fig. 3: Accessible values using the codification procedure (SLM_1 in blue, SLM_2 in red). The black dashed line delimits the useful values.

4. Results

Four different beams with arbitrary polarization and shape distributions have been considered. The first case (Fig. 4(a)) is a radially polarized beam. In the second, (Fig. 4(b)), the oscillation orientation changes according to the law $\theta(x,y) = 4\tan^{-1}(y/x)$. In these two cases, the shape $A_{sh}(x,y)$ remains constant. However, the illumination is not uniform due to the expanded Gaussian incident beam. The third case, (Fig. 4(c)), is a Laguerre-Gauss 10 mode (Eq. 2a), where the inner part of the beam is radially polarized and the external ring is azimuthally polarized. The last case considered, (Fig. 4(d)), is a doughnut-shaped beam following Eq. 2b; in this case the oscillation orientation and the phase delay are $\theta(x,y) = \tan^{-1}(y/x)$ and $\phi(x,y) = \pm 2\tan^{-1}(y/x)$ respectively. The $+$ sign stands for right-handed polarization states whereas the $-$ sign is used for left-handed cases.

$$A_{sh}(x,y) \propto \exp\left(-\frac{x^2+y^2}{w_0^2}\right) L_1^0\left(-\frac{x^2+y^2}{w_0^2}\right) \tag{2a}$$

$$A_{sh}(x,y) \propto (x^2+y^2)^{1/2} \exp\left(-\frac{x^2+y^2}{w_0^2}\right) \tag{2b}$$

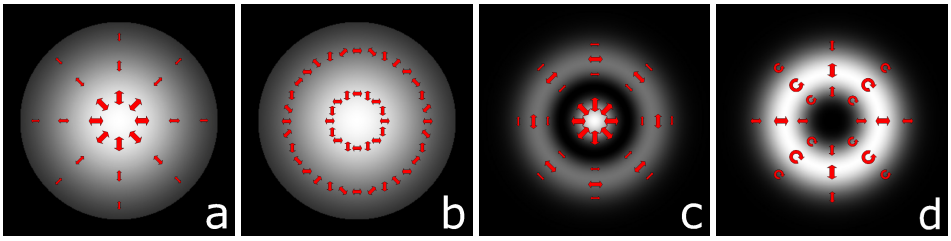

Fig. 4: (a) Gaussian beam with radial polarization, (b) Gaussian beam with 'star-like' polarization, (c) L_1^0 Laguerre-Gauss beam displaying different polarizations in the external ring and in the inner disc and (d) doughnut-shaped beam with $\phi(x,y) = \pm 2\tan^{-1}(y/x)$.

#183193 - $15.00 USD Received 17 Jan 2013; revised 15 Feb 2013; accepted 15 Feb 2013; published 26 Feb 2013

Note that w_0 is the beam waist radius and L_1^0 is the first generalized Laguerre polynomial. For the Laguerre-Gauss 10 and the doughnut-like cases, the effect of the input beam has been compensated for in the respective holograms. Four pairs of holograms have been calculated to generate the beams described above. The corresponding experimental light distributions obtained at the CCD plane are presented in Fig. 5. The first row shows the light distributions without analyzer P_2. Rows 2 to 5 display the results obtained for each beam when the analyzer P_2 is set at 0°, 45°, 90° and 135°, respectively.

The intensity patterns obtained clearly demonstrate that the synthesized beams behave as expected. Nevertheless, implementation requires us to deal with some non-critical drawbacks: (i) precise alignment of the different optical components is required, especially a good match between the corresponding pixels of the SLMs; (ii) the selected method requires the use of four-pixel cells to code each complex value, which means that the points available to define the wavefront are reduced by a factor of four; and (iii) some light is lost due to the modulation used (with a maximum transmittance $T = 0.4$, see Fig. 2).

To provide more insight about the method, an experimental measure of the Stokes parameters (S_0, S_1, S_2, S_3) (SP) has been carried out [21]. The beam used to perform this measure is a non-circular radially polarized Gaussian beam as shown in Fig. 6(a). In practice, these parameters are easily obtained according to the following relations

$$S_0 = I(0^\circ, 0) + I(90^\circ, 0) \tag{3a}$$
$$S_1 = I(0^\circ, 0) - I(90^\circ, 0) \tag{3b}$$
$$S_2 = I(45^\circ, 0) - I(135^\circ, 0) \tag{3c}$$
$$S_3 = I(45^\circ, \pi/2) - I(135^\circ, \pi/2)\,, \tag{3d}$$

where $I(\alpha, \beta)$ stands for the recorded intensity when the analyzer P2 is set at an angle α with respect to the x direction; β is the retardation between the x and y directions. Related to the SP, the degree of polarization P (DP) is

$$P = \frac{\sqrt{S_1^2 + S_2^2 + S_3^2}}{S_0}\,. \tag{4}$$

Figures 6(b) to 6(f) show the obtained normalized parameters and the DP. These five images are presented in false color using the jet colormap. S_0 (Fig. 6(b)) represents the total intensity. S_1 (Fig. 6(c)) displays red and blue pixels in those areas where the dominant polarization is in the x or y directions respectively. Note that the polarization direction changes smoothly, according to a radially polarized pattern. A similar interpretation is possible for S_2 (Fig. 6(d)) but for $\alpha = 45^\circ$ and $\alpha = 135^\circ$. S_3 (Fig. 6(e)), that compares the amount of right and left handed circular polarization of the field, is almost zero everywhere. Finally, the DP is shown in Fig. 6(f): notice that $P = 1$ for the points of the beam and is nearly zero outside.

#183193 - $15.00 USD Received 17 Jan 2013; revised 15 Feb 2013; accepted 15 Feb 2013; published 26 Feb 2013

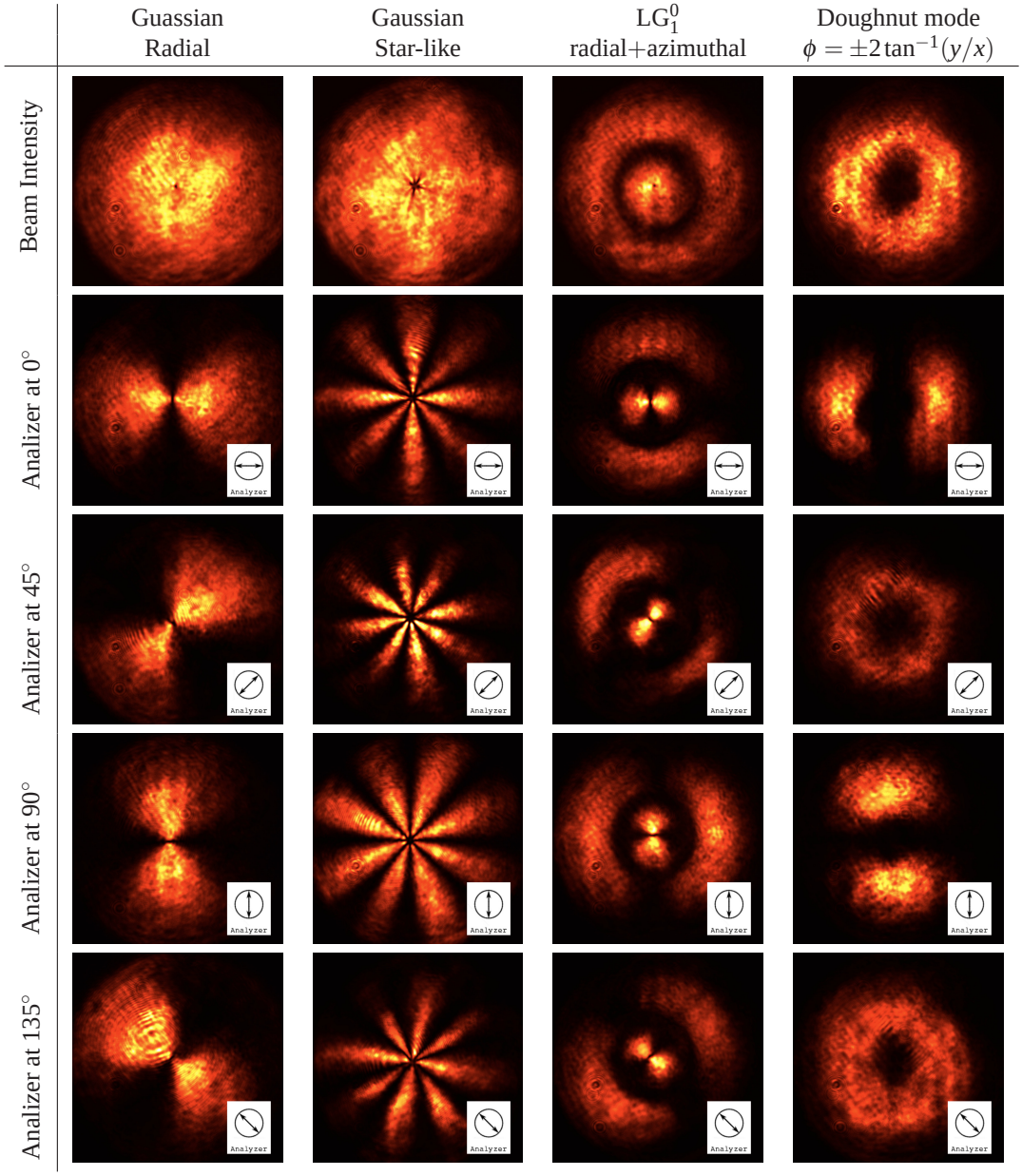

Fig. 5: Experimental intensity patterns for different positions of the analyzer P_2. All the experimental images were recorded using an 8-bit CCD and displayed in false color using the hot colormap to help assess the imperfections of the experimental beam.

#183193 - $15.00 USD Received 17 Jan 2013; revised 15 Feb 2013; accepted 15 Feb 2013; published 26 Feb 2013

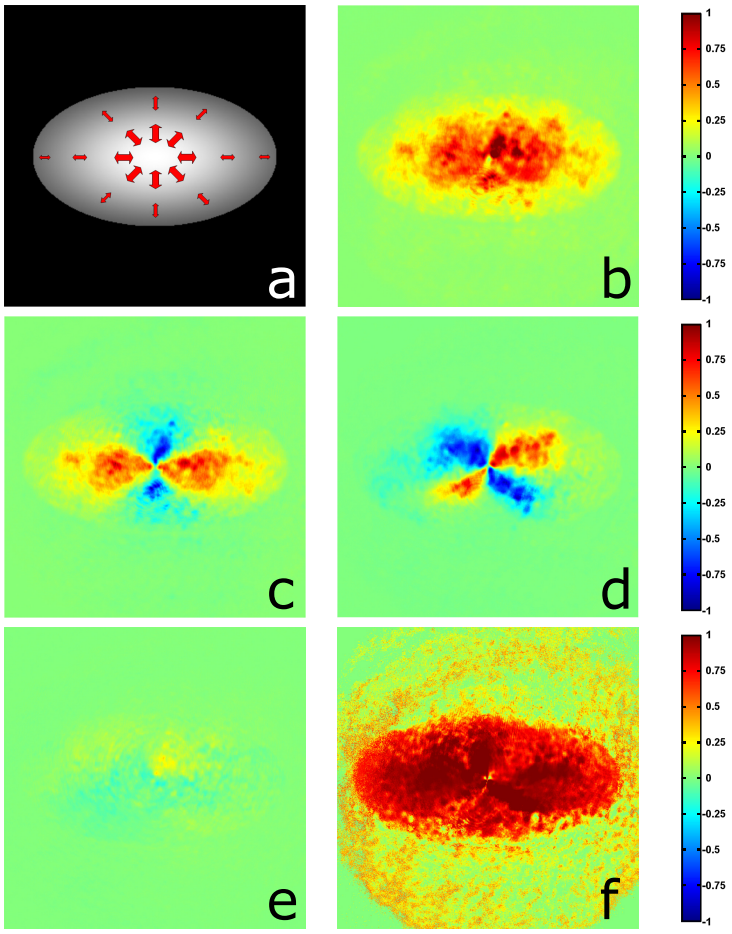

Fig. 6: Experimentally measured Stoke parameters: (a) Radially polarized elliptically-shaped Gaussian beam, (b) S_0, (c) S_1, (d) S_2, (e) S_4, (f) P.

5. Conclusions

Here we present a method for generating light beams with controlled polarization and shape using a Mach-Zehnder setup. The transverse components of the beam are manipulated independently through the use of transmissive liquid crystal displays in each arm of the interferometer. Since the devices used are not able to modulate the phase from 0 to 2π and present amplitude-phase coupling, a cell-oriented computer generated hologram algorithm has to be used to encode the information; in this way, full complex modulation can be achieved. Different beams with arbitrary polarization and shape distributions have successfully been obtained experimentally thereby demonstrating the feasibility of the proposed technique.

Acknowledgment

This work was funded in part by the Spanish Ministerio de Ciencia e Innovación, project FIS2010-17543.

#183193 - $15.00 USD Received 17 Jan 2013; revised 15 Feb 2013; accepted 15 Feb 2013; published 26 Feb 2013